Available online at www.sciencedirect.com
ScienceDirect
Trans. Nonferrous Met. Soc. China 32(2022) 2828−2837
Transactions of Nonferrous Metals Society of China
www.tnmsc.cn

Study on corrosion resistance of artificially aged 7075 aluminium alloy by using Cs-corrected STEM

Fang LIU[1,2], Jing-xu ZHENG[2,3], Xia CHEN[1], Xue-song XU[2], Bin CHEN[2]

1. State Key Laboratory of Refractories and Metallurgy, Wuhan University of Science and Technology, Wuhan 430081, China;
2. School of Materials Science and Engineering, Shanghai Jiao Tong University, Shanghai 200240, China;
3. Department of Materials Science and Engineering, Cornell University, NY 14853, USA

Received 23 November 2020; accepted 9 July 2021

Abstract: This research studied the mechanism of the corrosion resistance enhancement of artificially aged 7075 aluminium alloy using advanced Cs-corrected scanning transmission electron microscopy (STEM). The corrosion behaviors of artificially aged 7075 aluminium alloys in a 3.5 wt.% NaCl solution were investigated by impedance spectra, equivalent circuit analyses, polarization measurements and immersion tests. The results show that a longer aging treatment leads to better corrosion resistance, which can be attributed to the following microstructural features, as revealed by STEM. The Cu segregation at grain boundaries under over-aged conditions helps retard intergranular corrosion. The $Mg(Zn,Cu)_2$ precipitates formed on the surfaces of $Al_{18}Mg_3(Cr,Mn)_2$ dispersoids effectively insulate the dispersoids as cathodes in corrosion, from the Al matrix. This study demonstrates a potential strategy to design corrosion-resistant alloys achieved by proper alloying and subsequent aging.

Key words: 7075 aluminium alloy; artificial aging; $Mg(Zn,Cu)_2$ precipitate; intergranular corrosion; Cs-corrected scanning transmission electron microscopy

1 Introduction

7xxx series aluminium alloys, as a series of precipitation-hardenable alloys, have been widely used in aeronautical industries because of their high strength, light mass and excellent mechanical properties [1−3]. However, a limitation in the application of 7xxx alloys is that these alloys are susceptible to localized types of corrosion like pitting, intergranular corrosion and exfoliation corrosion, which may strongly reduce the service life of aerospace components, inducing a negative effect on safety and costs.

The microstructure of 7075 aluminium alloy is heterogeneous and consists of Al matrix, dispersoid particles, strengthening precipitates, precipitate-free zones (PFZ) near the grain boundaries and grain boundary precipitates (GBPs) [4−6]. The dispersion particles are formed by the addition of alloying elements (such as Cr and Mn) to the alloy. These particles are 0.1−0.2 μm in diameter and are homogeneously dispersed. The strengthening precipitates have a chemical composition of η-phase and size in the nanometer range [7]. Their precipitation in the matrix provides high strength during aging [8−10]. Owing to the difference in corrosion potentials, the particles or precipitates usually cause localized corrosion such as the pitting corrosion and intergranular corrosion. The dispersoids or precipitates, which are electrochemically nobler than the matrix, can act as effective cathodes initiating pitting corrosion, whereas those are more positive than cathodes. It is

Corresponding author: Bin CHEN, Tel: +86-21-54745404, E-mail: steelboy@sjtu.edu.cn
DOI: 10.1016/S1003-6326(22)65986-7

believed that the number, size and volume fraction of dispersoids remained unchanged during aging. Therefore, most researchers pay more attention to the influences of the precipitates evolution on corrosion behavior.

7xxx series aluminium alloys with T6 treatment are susceptible to localized corrosion and are prone to stress corrosion cracking. To improve their resistance to localized corrosion and stress corrosion cracking, over-ageing treatments such as T73, T74 and T76 have been developed [11−13]. Most researchers believe that the precipitate morphology plays a significant role in the corrosion of 7075 alloys. They focused on the role of matrix precipitates, PFZ, GBPs and grain boundary segregation as well as particles. MAITRA and ENGLISH [14] found that the over-aging treatment of 7075 alloys can decrease corrosion susceptibility. This is caused by not only the reduction in the potentials difference, but also the reduction in the amounts of solute atoms segregated. DEY et al [15] studied the differences in pitting severity in T6 and T73 tempers of AA7075 in 0.1 mol/L NaCl. In their studies, the differences in pit distribution can be explained by the role of particles and precipitates. ANDREATTA et al [4] investigated the initiation of localized corrosion during solution heat treatment, peak-aged (T6) and over-aged (T76) tempers of AA7075 alloy. They found that the localized corrosion of solution heat-treated AA7075 initiates at the intermetallics due to the high potential difference between the intermetallic and the matrix. The potential difference will decrease when the alloy is aged from the peak-aged (T6) temper to the over-aged (T7) temper. Besides, the intergranular corrosion is related to the precipitation of η-phase at the grain boundaries. WEI et al [16] observed the 7075-T6 alloys before and after immersion in a deaerated NaCl solution and found matrix dissolution around the Fe- and Mn-rich particles. They believed that the pitting corrosion was essentially attributable to these particles as a result of galvanic coupling between the particle and the matrix. In Ref. [17], JONES and HOEPPNER reported that a corrosion pit formed around the particle will cause a greater stress concentration than either the pit or the particle alone, which results in an aggravated corrosion attack. The influence of two novel aging treatments, T6I6 and high-temperature pre-precipitation aging on the intergranular corrosion of 7075 Al alloy was studied [18].

Although several researchers have investigated various microstructural features responsible for corrosion in 7075 alloys and developed many hypotheses, there has been a lack of general agreement on the origin and mechanism of corrosion.

STEM has been a powerful tool to characterize materials structures [19,20]. Cs-corrected STEM can render structure information at the atomic scale; while energy dispersive spectrum (EDS) can provide nano-scale compositional information. Herein, we comprehensively study the micro-structural evolution and the corrosion resistance evolution of 7075 alloys subjected to artificial aging. Based on Cs-corrected STEM and EDS, we show that the dispersoid particles, which can serve as cathodes in corrosion, are wrapped by $Mg(Zn,Cu)_2$ precipitates under over-aged conditions. In addition, the Cu segregation at grain boundaries retards intergranular corrosion. As a result, the corrosion resistance can be improved by the over-aging strategy.

2 Experimental

A commercial 7075 aluminium alloy plate with a thickness of 10 mm was used in this work, and the chemical composition is given in Table 1. Specimens were initially cut into the correct dimensions by wire-electrode cutting and then solution treated at 500 °C for 6 h, followed by water quenching at room temperature. To obtain different precipitation states of 7075 aluminium alloy, specimens were aged for different time, 0.5, 2, 4, 16, and 32 h, respectively.

Table 1 Chemical composition of 7075 alloy (wt.%)

Zn	Mg	Cu	Fe	Si	Mn	Cr	Ti	Al
5.47	2.54	1.44	0.45	0.33	0.22	0.22	0.15	Bal.

The Vicker microhardness machine (Buehler 1600−6406) was used to test the hardness of the specimens, and the test conditions were a load of 5 kg and a dwell time of 15 s. For each specimen, 5 test points were taken on the flat surface to calculate the average value as the final hardness and draw the aging curve. Electrochemical tests and immersion tests were carried out on the specimens

in these four stages.

Electrochemical test was conducted on an Ivium CompactStat electrochemical workstation. Pt was used as the auxiliary electrode, and a saturated calomel electrode (SCE) was used as the reference electrode. The specimens were immersed in 3.5 wt.% NaCl solution, then potentiodynamic polarization curves were measured and the EIS spectra were detected, respectively. The surface of each specimen for the electrochemical test was sealed with paraffin, with an uncovered area of 10 mm × 10 mm exposed. All electrochemical tests were performed after the open circuit potential (OCP) was stabilized. The potentiodynamic polarization measurements were performed by scanning the region at from −350 to 350 mV (vs SCE) with a scanning rate of 1 mV/s. The data were analyzed with the Ivium CompactState software. In the EIS measurements, alternating current (AC) voltage signal amplitude was 10 mV (peak to zero), and the frequency changed from 100 kHz to 10 MHz. The experimental data were analyzed using Z-view software.

Specimens were mechanically ground and polished for the measurement of the corrosion rate. The corrosion medium was 3.5 wt.% NaCl solution and the corrosion time was 7 d. The corrosion morphology and microstructure of the six 7075 specimens were investigated utilizing the SEM (JEOL JSM−7600F) equipped with EDS. The micrographs and the EDS spectra were obtained with an electron beam energy of 15 keV. The microstructure of 7075 alloys was characterized through a TEM (JEOL−ARM200F) to investigate the effect of the precipitates on the corrosion behavior of the alloy.

3 Results and discussion

3.1 Aging curve

Figure 1 shows the Vickers hardness curve of the 7075 aluminium alloy aged at 150 °C. The hardness evolution includes the under-aging stage, peak-aging stage, and over-aging stage, which is typical in heat-treatable aluminium alloy. In 7xxx aluminium alloys, three different types of strengthening precipitates are observed: GP zones, metastable precipitates (η') and equilibrium precipitates (η). The precipitation sequence is generally recognized as: GP zones→metastable precipitates η'→equilibrium precipitates η [7,21−23]. The GP zones are fine clusters of solute atoms, which are completely coherent with the matrix. The metastable precipitates η' are coherent or partially coherent with the matrix. The equilibrium precipitates η are larger than GP zones and metastable precipitates η' and are incoherent with the matrix. The stoichiometric composition of the equilibrium η phase is $MgZn_2$ [23]. GP zones and metastable η' precipitates serve as key strengthening structures [8,9].

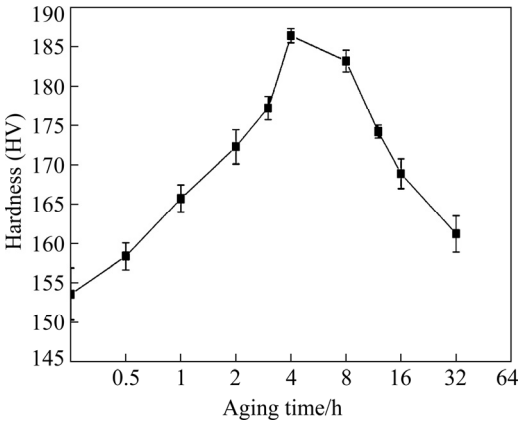

Fig. 1 Aging curve of 7075 aluminium alloy during isothermal aging at 150 °C

3.2 Precipitates in 7075 aluminium alloys

After being aged for different time, various precipitate states in 7075 aluminium alloys can be obtained. Figure 2 displays representative precipitation morphologies at different aging stages.

As seen in Fig. 2(a), there is no precipitate in the matrix in the micrograph of the solution-treated sample. As a result, the solution-treated specimen has comparatively low strength. The solution-treated specimen exhibits a large number of solute atoms (Mg and Zn) segregated at the grain boundaries [24]. Figure 2(b) and (c) show under-aged precipitate morphologies. A small number of GP zones and η' precipitates are embedded in the matrix. In HAADF-STEM mode, contrast variations result from the atomic number (Z) difference. Compared with Al, Mg has a lighter atomic number, which results in lower contrast. Zn has brighter contrast than Al due to its greater atomic number. Therefore, the center of the precipitate is attributed to Mg enrichment while the bright contrast on the edges of the precipitate is attributed to Zn enrichment [7]. At the peak-aging stage, Fig. 2(d) shows a very fine precipitate of η' in the matrix. The overall concentration of η' phases is

very high and their size is only a few nanometers at the peak-aging stage. Besides, several η phases are also observed as they have the brightest contrast due to η having a higher Zn/Mg molar ratio than GP zones and η' [22]. The micrographs in Figs. 2(e) and (f) indicate that a lot of η phases are present in the matrix for the over-ageing temper. Some of them grow to large sizes. Thus, peak-aged specimen exhibits higher strength than under-aged specimen and over-aged specimen.

3.3 Electrochemical properties

3.3.1 Electrochemical impedance spectroscopy

The EIS spectra, acquired at the OCP after a stabilization period, provide insights into the corrosion susceptibility of 7075 alloys in corrosive solution. The representative Nyquist diagrams registered from all the considered specimens and the equivalent circuit used to fit the EIS test data are depicted in Fig. 3(a).

It can be seen from Fig. 3(a) that the radius of the Nyquist loop increased significantly with the increasing aging time of specimens, indicating a better corrosion resistance of the alloy with increased aging time. A high-frequency depressed charge transfer semicircle is characteristic of solid electrodes and is often referred to as a frequency dispersion effect, which can be input to non-homogeneity and the rough-textured metal surface [25,26].

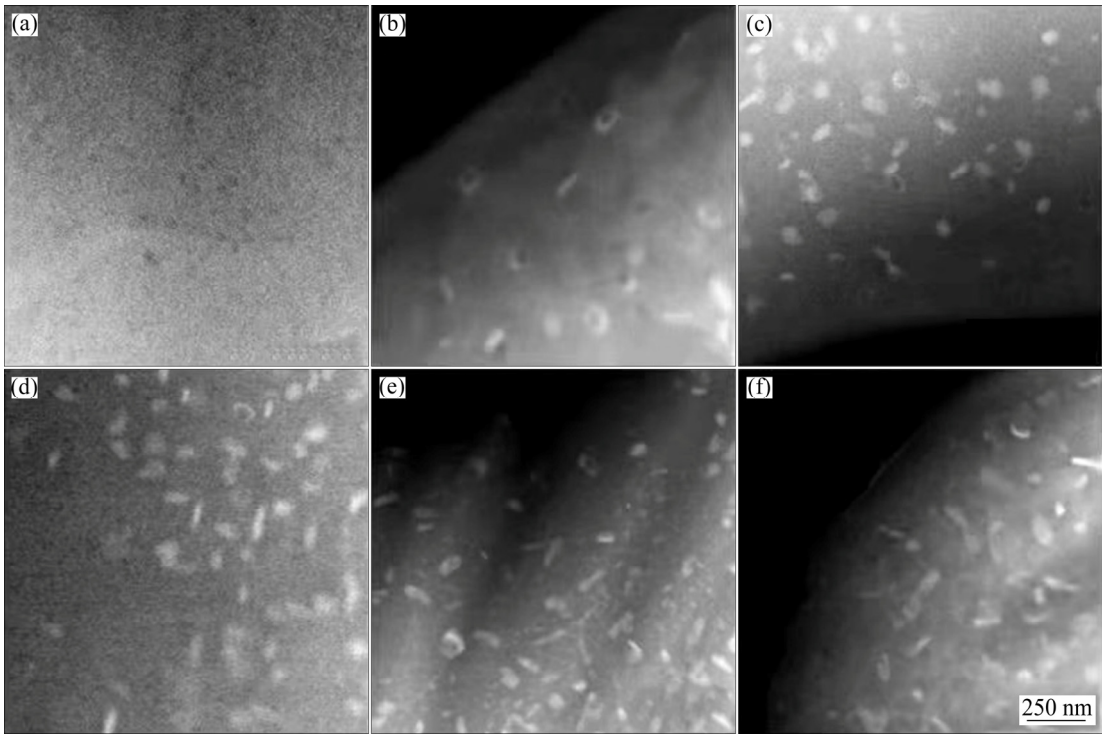

Fig. 2 HAADF-STEM images of 7075 aluminium alloy: (a) Solution-treated; (b) Aged for 0.5 h; (c) Aged for 2 h; (d) Aged for 4 h; (e) Aged for 16 h; (f) Aged for 32 h

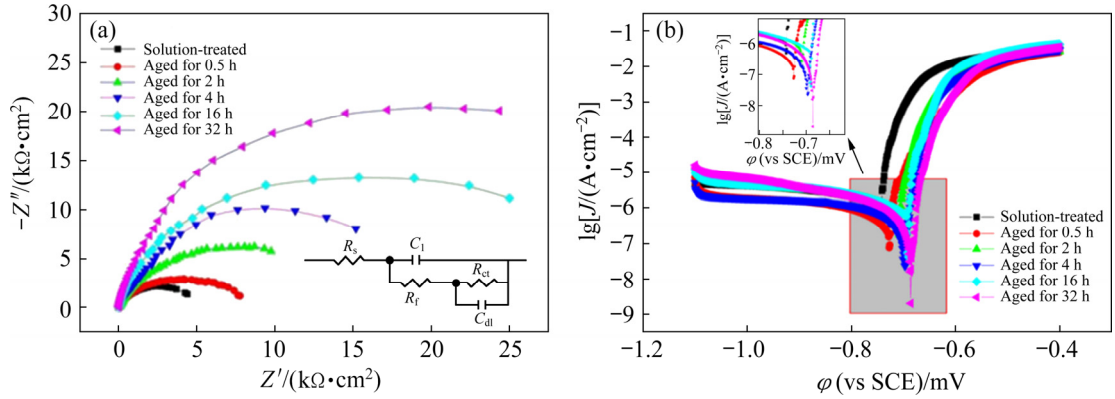

Fig. 3 Nyquist (a) and Tafel (b) plots for 7075 aluminium alloy in 3.5 wt.% NaCl solution

To reveal the effect of microstructure on corrosion behavior properly, an equivalent circuit as shown in Fig. 3(a) was applied to fitting the capacitive parts (≥0.1 Hz, above the real axis in Nyquist plot) of EIS spectra. The elements of the equivalent electrical circuit are as follows: R_s is the solution resistance, C_1 is associated with the original surface capacitance at high frequency, R_f is the high-frequency resistance corresponding to the resistance of electrolyte and corrosion products within the corrosion path (pores), R_{ct} is the charge transfer resistance on the active corroded surface in the low-frequency range, and C_{dl} associated with the interfacial capacitance of the new interface originated from NaCl solution, which is parallel to the charge transfer resistance in a low-frequency range. The relative error of the fit was obtained ($x^2<1\times10^{-2}$). In Table 2, the R_f^{error}, C_1^{error}, R_{ct}^{error} and C_{dl}^{error} represent the relative errors of R_f, C_1, R_{ct} and C_{dl}, respectively.

With increasing aging time there was an increase in the value of R_{ct} in 3.5 wt.% NaCl solution as shown in Table 2. The increase of R_{ct} values is attributed to the increase in resistance, which is in good agreement with the results from Nyquist diagrams.

3.3.2 Potentiodynamic polarization curves

The results of potentiodynamic polarization tests of the 7075 alloys after 10 min of OCP stabilization in 3.5 wt.% NaCl solution are shown in Fig. 3(b). To make the overlapping part of the 6 curves clearer, the partial enlarged detail is displayed at the top left corner of Fig. 3(b).

The corrosion potential (φ_{corr}), corrosion current density (J_{corr}), anodic (β_a) and cathodic (β_c) slopes obtained by the anodic and cathodic regions of the Tafel plots are shown in Table 3. Additionally, $\sigma(\varphi_{corr})$ and $\sigma(J_{corr})$ are the variances of the corrosion potential and corrosion current density, respectively. There were 6 sets of data in Table 3, which represented for 6 different aging time. The corrosion current density (J_{corr}) can be calculated by extrapolating the Tafel lines to the corrosion potential.

It can be seen from Table 3 that the corrosion potential (φ_{corr}) was very close to each other. φ_{corr} became more positive with the increasing aging time of the specimen. The existence of a more negative φ_{corr} for the solution treatment stage than for the other stages is due to the presence of a supersaturated solid solution of active Zn and Mg. Active Zn and Mg in solid solution tend to shift the

Table 2 Nyquist data and error values for 7075 aluminum alloys in 3.5 wt.% NaCl solution at 298 K for various aging time

Aging time/h	R_s/ ($\Omega\cdot cm^2$)	R_f/ ($\Omega\cdot cm^2$)	R_f^{error}/ %	C_1/ ($\mu F\cdot cm^{-2}$)	C_1^{error}/ %	R_{ct}/ ($\Omega\cdot cm^2$)	R_{ct}^{error}/ %	C_{dl}/ ($\mu F\cdot cm^{-2}$)	C_{dl}^{error}/ %
0	8.529	480.2	5.7566	6.1913	1.2099	3879	2.0783	5.5145	3.4056
0.5	13.08	469.3	3.5581	0.9709	1.4905	6198	1.8136	2.2663	2.4499
2	10.93	267.6	3.7071	1.5912	1.8252	10662	2.8215	4.2871	2.1902
4	7.981	508.3	6.9164	2.3117	2.0368	17513	4.8821	3.1545	3.6522
16	8.027	1138	8.6620	4.2112	1.1350	26366	2.7300	2.1547	3.8304
32	9.091	638	10.066	4.1085	1.2645	35516	3.7575	1.7605	4.0798

Table 3 Tafel polarization data for 7075 aluminium alloys in 3.5 wt.% NaCl solution for various aging time

Aging time/h	φ_{corr}(vs SCE)/mV	β_a/(mV·dec^{-1})	$-\beta_c$/(mV·dec^{-1})	J_{corr}/($\mu A\cdot cm^{-2}$)	$\sigma(\varphi_{corr})$	$\sigma(J_{corr})$
0	−0.7692	27	548	1.8770	0.01656	0.07043
0.5	−0.7522	45	532	0.8220	0.00362	0.01903
2	−0.7132	18	64	0.7180	0.00290	0.00591
4	−0.7050	19	228	0.4558	0.00245	0.00714
16	−0.6918	19	110	0.3411	0.00295	0.00146
32	−0.6895	18	99	0.2884	0.00045	0.00404

OCP(φ_{corr}) of the alloy in the negative direction [4]. The peak-aging and the over-aging cause a shift of φ_{corr} to more positive values compared to the solution treatment. This shift is more pronounced for the over-aging stage because a higher quantity of Zn and Mg precipitate from the solid solution during over-aging than those during peak-aging, under the measurement of microhardness. The corrosion current density (J_{corr}) decreases significantly with increasing aging time of the specimen, indicating that increasing aging time can effectively decrease the corrosion rate. Moreover, the corrosion current densities of the 6 specimens exhibit distinguished. The over-aged specimen has the lowest corrosion current density. As a result, the local anodic dissolution of the over-aged specimen may be slighter than the other specimens.

3.4 Immersion test results

Figure 4 indicates the exposed surface of 7075 alloys in 3.5 wt.% NaCl solution. The exposed surfaces present different levels of localized corrosion for various aging time. The localized attack in the exposed surface is severer for the solution-treated specimen than that for other specimens. With the increase of aging time, the corrosion resistance of 7075 alloys is improved.

3.5 Microstructures

To further investigate the effect of aging on the corrosion mechanism, the microstructure of aged specimens was observed by HAADF−STEM and EDS mapping. Figures 5(a), (b), and (c) display the HAADF−STEM images of the under-aged, peak-aged, and over-aged specimens, respectively, with their corresponding EDS mappings of elements Mg, Zn, Cu, Cr, and Mn. According to the EDS mapping analysis of the alloy, the dispersoids contain Cr and Mn. In all specimens, the Cr- and Mn-rich dispersoids are dispersed uniformly within the matrix grains or at the grain boundaries. In Fig. 5(a), the extremely fine η' precipitates are uniformly distributed in the matrix of the under-aged specimen. However, the GBPs have a larger size than the matrix precipitates. In the peak-aged specimen, the GBPs are coarse and distributed discontinuously at the grain boundary, as shown in Fig. 5(b). Additionally, the PFZ is also observed at the grain boundaries. In the over-aged specimen, although the size of GBPs remains unchanged, the discontinuous distribution of GBPs is almost replaced by the continuous distribution. Nevertheless, no significant variation in the PFZ width is noted. The improvement of corrosion resistance is shown not to be related to the PFZ width. The EDS analysis indicates that GBPs at the peak-aging stage contain Mg and Zn elements. Nevertheless, the over-aging treatment results in a relatively high localized concentration of Cu in GBPs. RAMGOPAL et al [27] reported that the Cu concentration in the GBSs of the T7 temper is seen to be much higher than that for the T6 temper in 7150 alloys, which makes the T7 temper more

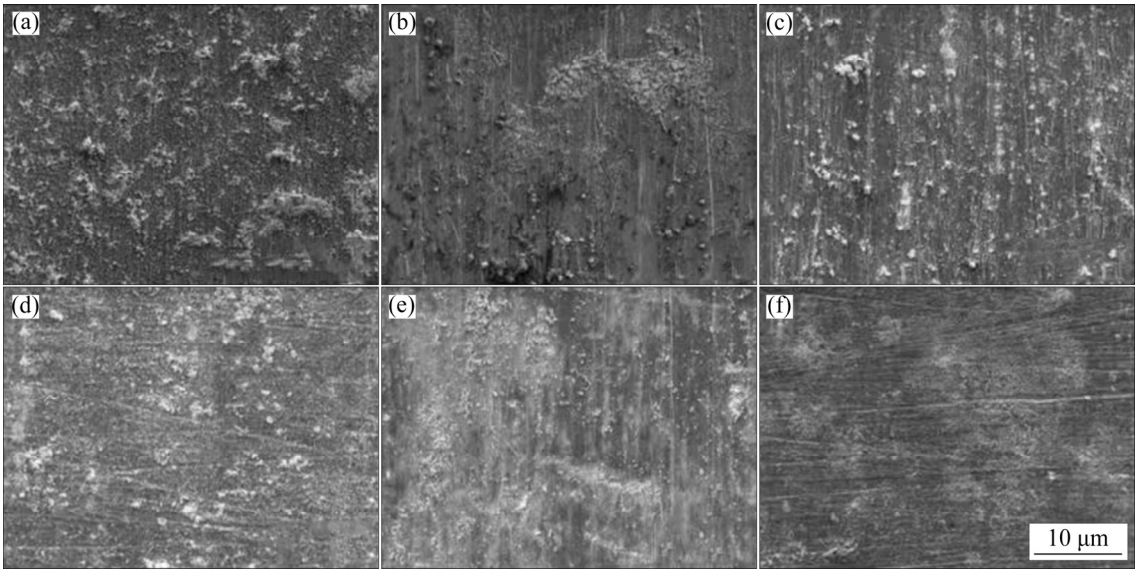

Fig. 4 SEM images of 7075 aluminium alloys in 3.5 wt.% NaCl solution for 7 d: (a) Solution-treated; (b) Aged for 0.5 h; (c) Aged for 2 h; (d) Aged for 4 h; (e) Aged for 16 h; (f) Aged for 32 h

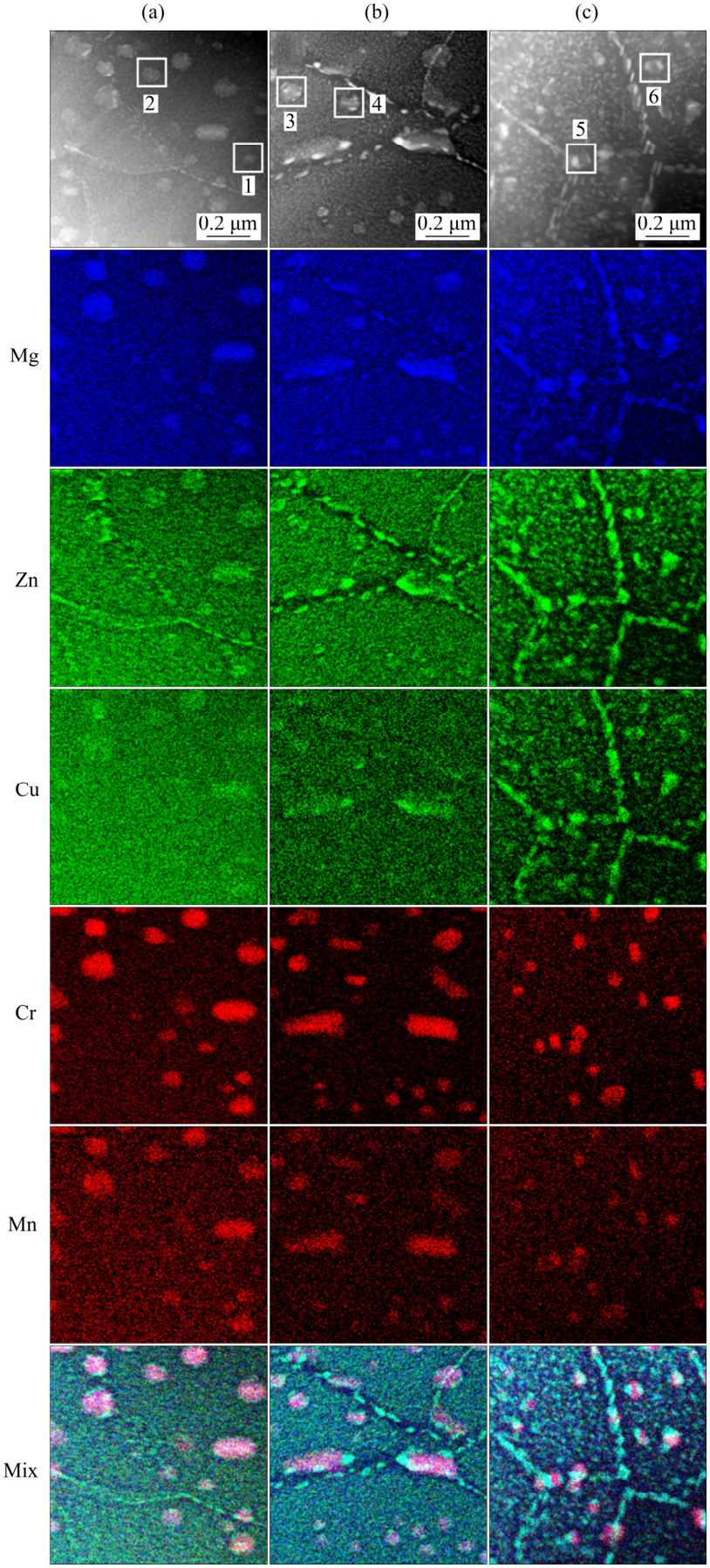

Fig. 5 HAADF−STEM images of precipitates at grain boundary of aged 7075 aluminium alloys and corresponding EDS mapping results: (a) Under-aged specimen (2 h); (b) Peak-aged specimen (4 h); (c) Over-aged specimen (16 h)

resistant to intergranular corrosion than the T6 temper.

It is interesting to find some precipitates form on the surface of Cr- and Mn-rich dispersoids. Figure 6 shows the atomic-resolution HAADF-STEM images of the Cr- and Mn-rich dispersoids and the precipitates on their surfaces, respectively. The atomic columns displayed in Figs. 6(a) and (b) coincide well with the crystal model view from the [110] direction of $Al_{18}Mg_3Cr_2$ and [11$\bar{2}$0] direction of $MgZn_2$, respectively. This provides strong evidence that, in consideration of the EDS mapping results, the Cr- and Mn-rich dispersoid is the $Al_{18}Mg_3(Cr,Mn)_2$ and the Zn-rich precipitate is the $Mg(Zn,Cu)_2$.

The variation of morphology and size of the precipitates on the surface of dispersoids is observed during aging treatment. Figure 7 shows the enlarged images from the selected Areas 1−6 of Fig. 5, indexed by 1−6, correspondingly. This figure illustrates the typical growing process of $Mg(Zn,Cu)_2$ on $Al_{18}Mg_3(Cr,Mn)_2$. During the early

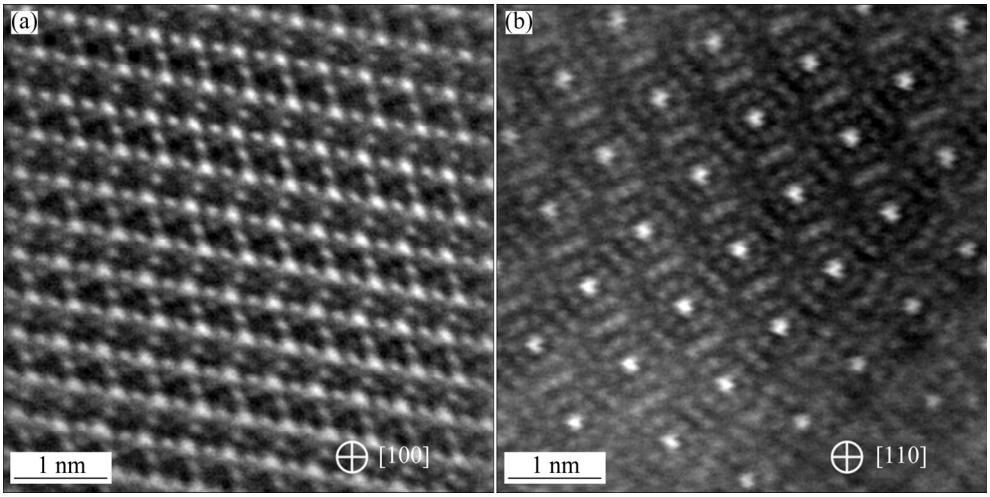

Fig. 6 Atomic-resolution HAADF-STEM images of $Al_{18}Mg_3(Cr,Mn)_2$ (a) and $Mg(Zn,Cu)_2$ (b)

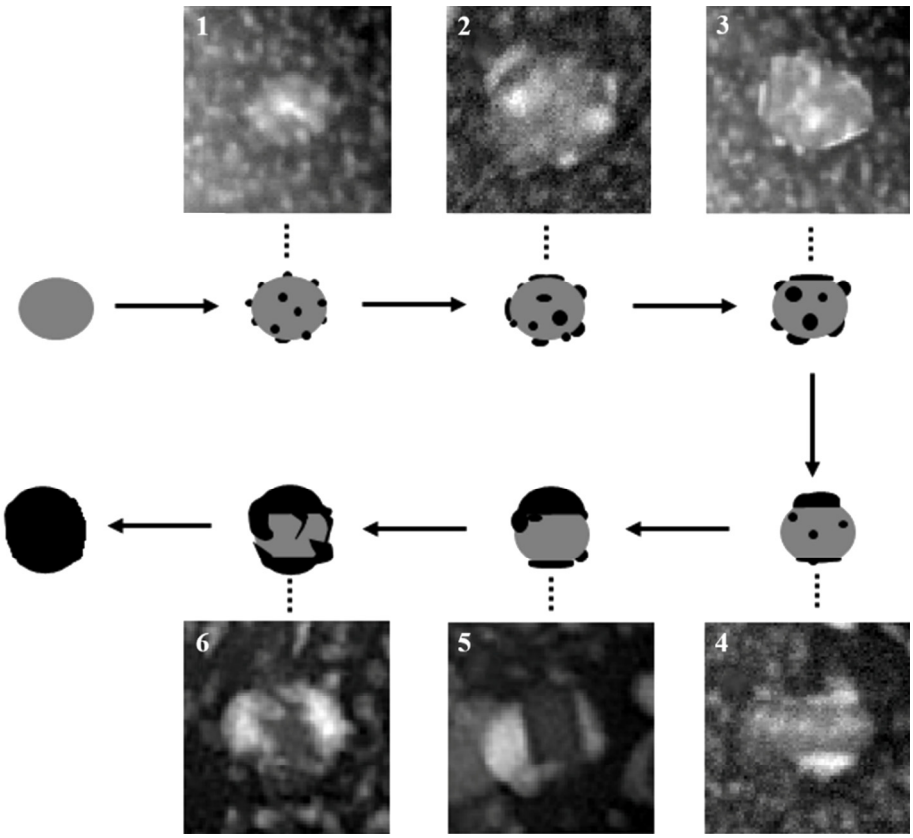

Fig. 7 Schematic diagram of precipitate−coating−dispersoid process

aging, the homogeneous nucleation of $Mg(Zn,Cu)_2$ on the surface of $Al_{18}Mg_3(Cr,Mn)_2$ is observed. As aging goes on, the precipitate size increases gradually while its density decreases. With further aging, whereas, the preferential growth along certain planes will occur. $Mg(Zn,Cu)_2$ will grow along other planes only if its thickness on preferential planes increases to a certain value.

The pitting corrosion was essentially attributable to dispersoids $Al_{18}Mg_3(Cr,Mn)_2$ as a result of galvanic coupling between the dispersoids and the matrix [17]. This is why the solution-treated specimen undergoes the severest corrosion attack. During aging treatment, the η-$Mg(Zn,Cu)_2$ precipitates form on the surface of $Al_{18}Mg_3(Cr,Mn)_2$ dispersoids, resulting in a decrease of the exposed surface. With the increase of aging time, the exposed surface of the $Al_{18}Mg_3(Cr,Mn)_2$ dispersoids decreases gradually. The $Mg(Zn,Cu)_2$ will coat $Al_{18}Mg_3(Cr,Mn)_2$ entirely if the aging time is long enough. The dispersoid $Al_{18}Mg_3(Cr,Mn)_2$ particles coated by $Mg(Zn,Cu)_2$ precipitates may have the same corrosion potentials as $Mg(Zn,Cu)_2$ in the matrix. As a result, the coated dispersoid particles exhibit similar electrochemical behaviors to the coarse $Mg(Zn,Cu)_2$ precipitates. POULOSE et al [28] suggest that the η' phases at the grain boundary can act as sacrificial anodes to retard intergranular corrosion cracking. This may also work in the case of dispersoid coated by $Mg(Zn,Cu)_2$. The precipitate coating on the dispersoid particles may likewise help to increase the resistance to pitting corrosion. The improvement of corrosion resistance of the alloy can, at least partially, be attributed to the coating process of dispersoid particles by precipitates.

4 Conclusions

(1) The corrosion resistance of 7075 aluminium alloy can be enhanced by artificial aging.

(2) The EDS analysis indicates that GBPs at the peak-ageing stage contain Mg and Zn. Nevertheless, the over-aging treatment results in a relatively high localized concentration of Cu in GBPs. Cu segregation at the grain boundaries can retard intergranular corrosion.

(3) During artificial aging, dispersoid particles, which can serve as cathodes in corrosion, are gradually wrapped by $Mg(Zn,Cu)_2$ precipitates. This wrapping process insulates the dispersoid particles from the Al matrix and thus may improve the corrosion resistance.

Acknowledgments

This research was supported by the Open Fund of the State Key Laboratory of Refractories and Metallurgy, China (No. G201907).

References

[1] SRIVATSAN T S, SRIRAM S, VEERARAGHAVAN D, VASUDEVAN V K. Microstructure, tensile deformation and fracture behaviour of aluminium alloy 7055 [J]. Journal of Materials Science, 1997, 32(11): 2883−2894.

[2] WILLIAMS J C, STARKE E A Jr. Progress in structural materials for aerospace systems [J]. Acta Materialia, 2003, 51(19): 5775−5799.

[3] HU Hui-e, ZHEN Liang, YANG Li, SHAO Wen-zhu, ZHANG Bao-you. Deformation behavior and microstructure evolution of 7050 aluminum alloy during high temperature deformation [J]. Materials Science and Engineering A, 2008, 488(1/2): 64−71.

[4] ANDREATTA F, TERRYN H, de WIT J H W. Corrosion behaviour of different tempers of AA7075 aluminium alloy [J]. Electrochimica Acta, 2004, 49(17/18): 2851−2862.

[5] AYER R, KOO J Y, STEEDS J W, PARK B K. Microanalytical study of the heterogeneous phases in commercial Al−Zn−Mg−Cu alloys [J]. Metallurgical and Materials Transactions A, 1985, 16(11): 1925−1936.

[6] HILL J A, MARKLEY T, FORSYTH M, HOWLETT P C, HINTON B R W. Corrosion inhibition of 7000 series aluminium alloys with cerium diphenyl phosphate [J]. Journal of Alloys and Compounds, 2011, 509(5): 1683−1690.

[7] ZHENG Jing-xu, LI Zhi, LUO Rui-chun, CHEN Bin. Precipitation in an Al−Zn−Mg−Cu alloy during isothermal aging: Atomic-scale HAADF-STEM investigation [J]. Materials Science and Engineering A, 2017, 691: 60−70.

[8] PARK J K, ARDELL A J. Microstructures of the commercial 7075 Al alloy in the T651 and T7 tempers [J]. Metallurgical and Materials Transactions A, 1983, 14(10): 1957−1965.

[9] PARK J K, ARDELL A J. Precipitate microstructure of peak-aged 7075 Al [J]. Scripta Metallurgica, 1988, 22(7): 1115−1119.

[10] ABREU C M, CRISTÓBAL M J, FIGUEROA R, PENA G. Wear and corrosion performance of two different tempers (T6 and T73) of AA7075 aluminium alloy after nitrogen implantation [J]. Applied Surface Science, 2015, 327(4): 51−61.

[11] OU Bin-lung, YANG Ji-gang, YANG Chen-kuo. Effects of step-quench and aging on mechanical properties and resistance to stress corrosion cracking of 7050 aluminum alloy [J]. Materials Transactions JIM, 2000, 41(7): 783−789.

[12] SPEIDEL M O. Stress corrosion cracking of aluminum alloys [J]. Metallurgical Transactions A, 1975, 6(4): 631−651.

[13] DAVIS J R. Corrosion of aluminum and aluminum alloys [M]. Washington: ASM International, 1999.
[14] MAITRA S, ENGLISH G C. Mechanism of localized corrosion of 7075 alloy plate [J]. Metallurgical Transactions A, 1981, 12(3): 535−541.
[15] DEY S, GUNJAN M K, CHATTORAJ I. Effect of temper on the distribution of pits in AA7075 alloys [J]. Corrosion Science, 2008, 50(10): 2895−2901.
[16] WEI R P, LIAO C M, GAO M. A transmission electron microscopy study of constituent-particle-induced corrosion in 7075-T6 and 2024-T3 aluminum alloys [J]. Metallurgical and Materials Transactions A, 1998, 29(4): 1153−1160.
[17] JONES K, HOEPPNER D W. The interaction between pitting corrosion, grain boundaries, and constituent particles during corrosion fatigue of 7075-T6 aluminum alloy [J]. International Journal of Fatigue, 2009, 31(4): 686−692.
[18] LI Jin-eng, PENG Zhuo-wei, LI Chao-xing, JIA Zhi-qiang, CHEN Wen-jing, ZHENG Zi-qiao. Mechanical properties, corrosion behaviors and microstructures of 7075 aluminium alloy with various aging treatments [J]. Transactions of Nonferrous Metals Society of China, 2008, 18(4): 755−762.
[19] ZHENG Jing-xu, LUO Rui-chun, ZENG Xiao-qin, CHEN Bin. Nano-scale precipitation and phase growth in Mg−Gd binary alloy: An atomic-scale investigation using HAADF-STEM [J]. Materials & Design, 2018, 137: 316−324.
[20] ZHENG Jing-xu, LI Zhi, LUO Rui-chun, XU Xue-song, CHEN Bin. Precipitation in Mg–Nd–Y–Zr–Ca alloy during isothermal aging: A comprehensive atomic−scaled study by means of HAADF-STEM [J]. Advanced Engineering Materials, 2017, 19(2): 1−9.
[21] MONDOLFO L F. Structure of the aluminium−magnesium−zinc alloys [J]. Metallurgical Reviews, 1971, 16(1): 95−124.
[22] HANSEN V, STILLER K, WATERLOO G, GJØNNES J, LI X Z. Structures and transformations during artificial aging of an industrial 7xxx-series Al−Zn−Mg−Zr alloy [J]. Materials Science Forum, 2002, 396/397/398/399/400/401/402: 815−820.
[23] BERG L K, GJØNNES J, HANSEN V, LI X Z, KNUTSON-WEDEL M, WATERLOO G, SCHRYVERS D, WALLENBERG L R. GP-zones in Al−Zn−Mg alloys and their role in artificial aging [J]. Acta Materialia, 2001, 49(17): 3443−3451.
[24] SONG R G, TSENG M K, ZHANG B J, LIU J, JIN Z H, SHIN K S. Grain boundary segregation and hydrogen-induced fracture in 7050 aluminium alloy [J]. Acta Materialia, 1996, 44(8): 3241−3248.
[25] ABBOUD Y, ABOURRICHE A, AINANE T, CHARROUF M, BENNAMARA A, TANANE O, HAMMOUTI B. Corrosion inhibition of carbon steel in acidic media by bifurcaria bifurcata extract [J]. Chemical Engineering Communications, 2009, 196(7): 788−800.
[26] LEBRINI M, ROBERT F, LECANTE A, ROOS C. Corrosion inhibition of C38 steel in 1 M hydrochloric acid medium by alkaloids extract from Oxandra asbeckii plant [J]. Corrosion Science, 2011, 53(2): 687−695.
[27] RAMGOPAL T, GOUMA P I, FRANKEL G S. Role of grain-boundary precipitates and solute-depleted zone on the intergranular corrosion of aluminum alloy 7150 [J]. Corrosion, 2002, 58(8): 687−697.
[28] POULOSE P K, MORRAL J E, MCEVILY A J. Stress corrosion crack velocity and grain boundary precipitates in an Al−Zn−Mg alloy [J]. Metallurgical and Materials Transactions B, 1974, 5(6): 1393−1400.

用球差校正扫描透射电镜研究人工时效 7075 铝合金的耐蚀性

刘 芳[1,2]，郑景旭[2,3]，陈 霞[1]，许雪松[2]，陈 彬[2]

1. 武汉科技大学 省部共建耐火材料与冶金国家重点实验室，武汉 430081；
2. 上海交通大学 材料科学与工程学院，上海 200240；
3. Department of Materials Science and Engineering, Cornell University, NY 14853, USA

摘 要：使用先进的球差校正扫描透射电子显微镜研究人工时效 7075 铝合金耐腐蚀性增强机制。通过阻抗谱、等效电路分析、极化测量和浸泡试验，研究人工时效 7075 铝合金在 3.5% (质量分数) NaCl 溶液中的腐蚀行为。结果表明，人工时效时间越长，7075 铝合金的耐腐蚀性越好。这可能归因于扫描透射电镜技术揭示的以下显微组织特征：在过时效条件下，晶界处的铜偏析有助于延缓晶间腐蚀，在 $Al_{18}Mg_3(Cr,Mn)_2$ 分散体表面形成的 $Mg(Zn,Cu)_2$ 沉淀有效地将作为腐蚀阴极的分散体与铝基体隔离。这项研究证明，可以通过适当的合金化和人工时效来设计耐腐蚀合金的可能性。

关键词：7075 铝合金；人工时效；$Mg(Zn,Cu)_2$ 析出相；晶间腐蚀；球差校正扫描透射电子显微镜

(Edited by Wei-ping CHEN)